NON-DARCY FULLY DEVELOPED MIXED CONVECTION IN A POROUS MEDIUM CHANNEL WITH HEAT GENERATION/ABSORPTION AND HYDROMAGNETIC EFFECTS

Ali J. Chamkha
Department of Mechanical and Industrial Engineering, Kuwait University, Safat, 13060 Kuwait

Volume-averaged equations are developed governing steady, laminar, fully developed, hydromagnetic mixed convection non-Darcian flow of an electrically conducting and heat-generating / absorbing fluid in a channel embedded in a uniform porous medium. Proper dimensionless parameters are employed for various thermal boundary conditions on the left and right walls of the channel prescribed as isothermal-isothermal, isothermal-isoflux, and isoflux-isothermal. Analytical expressions for the velocity and temperature profiles in the channel as well as for the mass flow rate, friction factor, and heat carried out by the fluid in the channel are developed for special cases of the problem. Conditions for the occurrence of fluid backflow zones are reported. The fully nonlinear governing equations are solved numerically by an implicit finite difference method. Favorable comparisons with the developed analytical results and previously published work are performed. Graphical results of the closed-form and numerical results are reported for various parametric conditions to illustrate special features of the solution.

INTRODUCTION

Mixed convection flow of an electrically conducting and heat-generating/absorbing fluid in a porous medium channel in the presence of a magnetic field is of special technical significance because of its frequent occurrence in many industrial applications such as geothermal reservoirs, cooling of nuclear reactors, thermal insulation, and petroleum reservoirs. There has been considerable published work dealing with free, forced, and mixed convection problems of different geometries embedded in porous and nonporous media in the presence and absence of a magnetic field [e.g., 1–15]. In analyzing and studying flows in porous media, Darcy's law is frequently employed. There is an empirical relation between the pressure drop across the porous medium and the viscous and gravitational forces. Minkowcyz et al. [16, 17] have reported solutions for mixed convection about a horizontal heated surface in a fluid-saturated porous medium [16] and about nonisothermal cylinders and spheres in porous media [17] using Darcy's law. Vafai and Tien [18, 19], Hong et al. [20], and Plumb and Huenefeld [21] discussed the

Received 8 January 1997; accepted 10 June 1997.
Address correspondence to Professor Ali J. Chamkha, Department of Mechanical and Industrial Engineering, Kuwait University, P.O. Box 5969, Safat, 13060 Kuwait. E-mail: chamkha@kuc01.kuniv.edu.kw

Numerical Heat Transfer, Part A, 32:653–675, 1997

1040–7782/97 $12.00 + .00

NOMENCLATURE

A	inverse Darcy number ($=w^2\varepsilon/K$)	$\bar{u}_p$	dimensional average fluid velocity in x direction
B_0	magnetic induction	U	dimensionless fluid velocity in X direction [$=u_p w/(\nu\ \mathrm{Gr})$]
c_p	fluid specific heat at constant pressure	U_{avg}	dimensionless average fluid velocity in X direction, defined by Eq. (19)
C	porous medium inertia coefficient	v_p	dimensional fluid velocity in y direction
Ec	Eckert number $\{=\nu^2\ \mathrm{Gr}^2/[w^2 c_p(T_L - T_\infty)]\}$	w	channel width
f	friction factor, defined by Eq. (22)	x	dimensional streamwise distance
g	gravitational acceleration	X	dimensionless streamwise distance [$=x/(w\ \mathrm{Gr})$]
Gr	Grashof number, defined in Table 1	y	dimensional transverse distance
H	dimensionless heat generaton or absorption [$=Q_0 w^2/(\rho\nu c_p)$]	Y	dimensionless transverse distance ($=y/w$)
k_e	effective thermal conductivity of porous medium	α_e	effective thermal diffusivity of porous medium [$=k_e/(\rho c_p)$]
K	permeability of porous medium	β	volumetric thermal expansion coefficient
m_p	dimensionless mass flow rate, defined by Eq. (18)	Γ	dimensionless porous medium inertia coefficient
M	Hartmann number [$=\sqrt{\sigma/(\rho\nu)}\ B_0 w$]	ε	porosity of porous medium
$\bar{p}$	dimensional difference between static and hydrostatic fluid pressures	ν	fluid kinematic viscosity
P	dimensionless difference between static and hydrostatic pressures [$=\bar{p}w^2/(\rho\nu^2\ \mathrm{Gr}^2)$]	ρ	fluid density
Pr	Prandtl number ($=\nu/\alpha_e$)	σ	fluid electrical conductivity
q	dimensional heat flux	τ_T	ratio of left to right wall temperatures ($=\phi_L/\phi_R$)
Q	dimensionless heat flux, defined in Table 1	ϕ	dimensionless fluid temperature
Q_f	dimensionless heat carried out by fluid, defined by Eq. (24)	**Subscripts**	
Q_0	dimensional heat generation or absorption (>0)		
Re	Reynolds number ($=\bar{u}_p w/\nu$)		
T	dimensional fluid temperature	L	left wall of channel
u_p	dimensional fluid velocity in x direction	R	right wall of channel
		∞	ambient reference quantity

effects of the presence of a boundary adjacent to a porous medium and the inertial effects that would occur when the velocity in the porous medium becomes high (that is, the Reynolds number based on the mean pore size is greater than unity). In this case, the pressure gradient across the porous medium is a quadratic relation with the volume-averaged velocity. In addition to the boundary and inertia effects, often called non-Darcy effects, mentioned above, nonuniform porosity effects are employed by Hong et al. [20] in analyzing vertical plate natural convection flow in porous media.

The study of heat generation or absorption effects in moving fluids is important in view of several physical problems such as those dealing with chemical reactions and those concerned with dissociating fluids (see [22, 23]). Also, the design of placing many electronic circuits into one small chip and more chips into a

package results in high volumetric heat generation in the electronic equipment (see [10]). This led to the consideration of heat generation effects in porous media. Recently, Chamkha [24] analyzed the problem of non-Darcy free convection flow about a wedge and a cone embedded in a porous medium in the presence of heat generation effects. Other works dealing with heat generation effects can be found in some of the references of the paper by Vajravelu and Hadjinicolaou [22].

The purpose of this article is to consider non-Darcy fully developed mixed convection flow in a channel embedded in a porous medium (called herein a porous medium channel) in the presence of heat generation/absorption and hydromagnetic effects. Several thermal boundary conditions prescribed as isothermal-isothermal, isothermal-isoflux, and isoflux-isothermal will be investigated in the present work.

GOVERNING EQUATIONS

Consider fully developed, laminar, steady mixed convection flow of an electrically conducting and heat-generating/absorbing fluid in a vertical porous medium channel in the presence of a transverse magnetic field applied normal to the flow direction (see Figure 1). The fluid is assumed to be incompressible with constant properties except the density in the buoyancy term in the momentum equation. The magnetic Reynolds number is assumed to be small, so that the induced magnetic field is neglected and the Hall effect of magnetohydrodynamics is assumed to be negligible. The governing equations for this investigation are based on the usual balance laws of mass, linear momentum, and energy modified to account for combined boundary and inertia effects of porous media, buoyancy effects, and hydromagnetic and heat generation or absorption effects. These can be

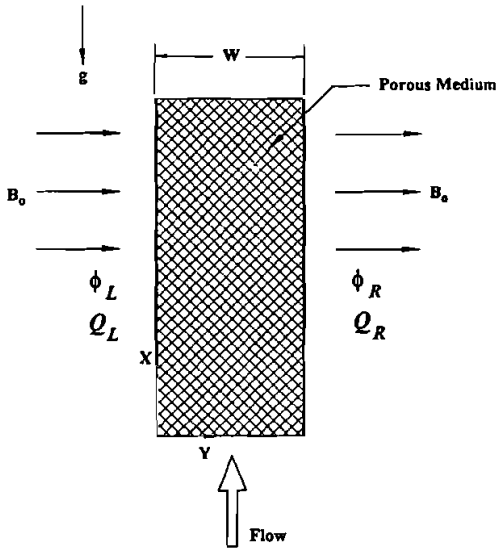

Figure 1. Schematic of the porous medium channel.

written as

$$\frac{\partial u_p}{\partial x} + \frac{\partial v_p}{\partial y} = 0 \tag{1}$$

$$\frac{\nu\varepsilon}{K} u_p + C\varepsilon^2 u_p |u_p| + u_p \frac{\partial u_p}{\partial x} + v_p \frac{\partial u_p}{\partial y}$$

$$= g\beta(T - T_\infty) + \nu \frac{\partial^2 u_p}{\partial y^2} - \frac{1}{\rho} \frac{d\bar{p}}{dx} - \frac{\sigma B_0^2}{\rho} u_p \tag{2}$$

$$u_p \frac{\partial T}{\partial x} + v_p \frac{\partial T}{\partial y} = \alpha_e \frac{\partial^2 T}{\partial y^2} \pm \frac{Q_0}{\rho c_p}(T - T_\infty) + \frac{\sigma B_0^2}{\rho c_p} u_p^2 \tag{3}$$

where $\bar{p}$ is the difference between static and hydrostatic pressures. All other parameters are defined in the Nomenclature. The physics of the problem suggests the following boundary conditions:

$$u_p(x,0) = 0 \qquad v_p(x,0) = 0 \qquad T(x,0) = T_L \qquad -k_e \frac{\partial T}{\partial y}(x,0) = q_L \tag{4}$$

$$u_p(x,w) = 0 \qquad v_p(x,w) = 0 \qquad T(x,w) = T_R \qquad -k_e \frac{\partial T}{\partial y}(x,w) = q_R \tag{5}$$

Since the flow is fully developed, the fluid velocity components will no longer be dependent on the axial distance x. This causes Eq. (1) to give $\partial v_p/\partial y = 0$. Application of either $v_p(x,0) = 0$ of Eq. (4) or $v_p(x,w) = 0$ of Eq. (5) will yield $v_p = 0$ everywhere. Using this result and employing the proper dimensionless quantities given in the Nomenclature and Table 1 for the different types of thermal boundary conditions, the following dimensionless equations and boundary conditions result:

$$\phi = \frac{dP}{dX} - \frac{d^2U}{dY^2} + AU + \Gamma U|U| + M^2 U \tag{6}$$

$$U \,\mathrm{Pr} \frac{\partial \phi}{\partial X} = \frac{\partial^2 \phi}{\partial Y^2} \pm \mathrm{Pr}\, H\phi + \mathrm{Pr}\,\mathrm{Ec}\, M^2 U^2 \tag{7}$$

$$U(0) = 0 \qquad \phi(0) = \phi_L \qquad \frac{\partial \phi(0)}{\partial Y} = -Q_L \tag{8}$$

$$U(1) = 0 \qquad \phi(1) = \phi_R \qquad \frac{\partial \phi(1)}{\partial Y} = -Q_R \tag{9}$$

Table 1. Nondimensional variables and parameters

	$T_L - T_R$		$T_L - q_R$		$q_L - T_R$	
	Left wall	Right wall	Left wall	Right wall	Left wall	Right wall
ϕ	$\frac{T - T_\infty}{T_L - T_\infty}$	$\frac{T - T_\infty}{T_R - T_\infty}$	$\frac{T - T_\infty}{T_L - T_\infty}$	$\frac{k_e(T - T_\infty)}{q_R w}$	$\frac{k_e(T - T_\infty)}{q_L w}$	$\frac{T - T_\infty}{T_R - T_\infty}$
Q	$\frac{qw}{k_e(T_L - T_\infty)}$	$\frac{qw}{k_e(T_R - T_\infty)}$	$\frac{qw}{k_e(T_L - T_\infty)}$	$\frac{q}{q_R}$	$\frac{q}{q_L}$	$\frac{qw}{k_e(T_R - T_\infty)}$
Gr	$\frac{g\beta(T_L - T_\infty)w^3}{\nu^2}$	$\frac{g\beta(T_R - T_\infty)w^3}{\nu^2}$	$\frac{g\beta(T_L - T_\infty)w^3}{\nu^2}$	$\frac{g\beta q_R w^4}{k_e \nu^2}$	$\frac{g\beta q_L w^4}{k_e \nu^2}$	$\frac{g\beta(T_E - T_\infty)w^3}{\nu^2}$
ϕ_L	1	$\frac{T_L - T_\infty}{T_R - T_\infty}$	1	$\frac{k_e(T_L - T_\infty)}{q_R w}$	—	—
ϕ_R	$\frac{T_R - T_\infty}{T_L - T_\infty}$	1	—	—	$\frac{k_e(T_R - T_\infty)}{q_L w}$	1
Q_L	—	—	—	—	1	$\frac{q_L w}{k_e(T_R - T_\infty)}$
Q_R	—	—	$\frac{q_R w}{k_e(T_L - T_\infty)}$	1	—	—

Equations (6)–(9) are nonlinear and possess no closed-form solution and therefore must be solved numerically. However, if the nonlinear terms are neglected in comparison with the remaining linear terms, the problem can then be solved analytically. The possible analytical solutions are presented next.

ANALYTICAL RESULTS

For slow flow in the porous medium the porous medium non-Darcian inertial parameter Γ, which represents the additional pressure loss resulting from interpore mixing existing at high velocities, can be neglected. In addition, if the fluid temperature gradient along the axial distance X is neglected, that is, the fluid temperature is uniform along the X direction, as is the case for the various thermal boundary conditions prescribed as isothermal-isothermal, isothermal-isoflux, and isoflux-isothermal, and if the magnetic dissipation effect is neglected, analytical solutions to the governing equations are possible. Setting $\Gamma = 0$, Ec = 0, and $\partial\phi/\partial X = 0$ in Eqs. (6) and (7) and rearranging yields

$$\frac{d^2U}{dY^2} - (A + M^2)U = \frac{dP}{dX} - \phi \tag{10}$$

$$\frac{d^2\phi}{dY^2} \pm \mathrm{Pr}\, H\phi = 0 \tag{11}$$

It should be mentioned that the form of the analytical solution for ϕ is different for a heat-generating fluid [positive sign in Eq. (11)] than for a heat-absorbing fluid [negative sign in Eq. (11)]. Closed-form solutions will be developed for these two cases.

Heat-Generating Fluid (Source)

For this type of fluid the energy equation, Eq. (11), with the positive sign in the second term is a linear differential equation that has the following closed-form solution for ϕ:

$$\phi = C_1 \cos\sqrt{\mathrm{Pr}\,H}\,Y + C_2 \sin\sqrt{\mathrm{Pr}\,H}\,Y \tag{12}$$

where C_1 and C_2 are arbitrary constants determined by the thermal boundary conditions. It can be shown that

$$C_1 = \phi_L \qquad C_2 = \frac{\phi_R - \phi_L \cos\sqrt{\mathrm{Pr}\,H}}{\sin\sqrt{\mathrm{Pr}\,H}} \tag{13}$$

for the isothermal-isothermal condition,

$$C_1 = \phi_L \qquad C_2 = \frac{-Q_R + \sqrt{\mathrm{Pr}\,H}\,\phi_L \sin\sqrt{\mathrm{Pr}\,H}}{\sqrt{\mathrm{Pr}\,H}} \tag{14}$$

for the isothermal-isoflux condition, and

$$C_1 = \frac{\phi_R + \left(Q_L/\sqrt{\mathrm{Pr}\,H}\right)\sin\sqrt{\mathrm{Pr}\,H}}{\cos\sqrt{\mathrm{Pr}\,H}} \qquad C_2 = \frac{-Q_L}{\sqrt{\mathrm{Pr}\,H}} \tag{15}$$

for the isothermal-isoflux condition.

With the solution for ϕ determined, Eq. (10) can be solved for U subject to the no-slip boundary conditions given by $U(0) = 0$ in Eqs. (8) and $U(1) = 0$ in Eq. (9). Without going into detail, it can be shown that U takes the form

$$U = B + D\cos\sqrt{\mathrm{Pr}\,H}\,Y + E\sin\sqrt{\mathrm{Pr}\,H}\,Y + C_3\cosh\sqrt{A + M^2}\,Y + C_4\sinh\sqrt{A + M^2}\,Y \tag{16}$$

where

$$B = \frac{-dP/dX}{(A + M^2)} \qquad D = \frac{C_1}{\mathrm{Pr}\,H + A + M^2} \qquad E = \frac{C_2}{\mathrm{Pr}\,H + A + M^2}$$

$$C_3 = -B - D \qquad C_4 = \frac{C_3\cosh\sqrt{A + M^2} + B + D\cos\sqrt{\mathrm{Pr}\,H} + E\sin\sqrt{\mathrm{Pr}\,H}}{-\sinh\sqrt{A + M^2}} \tag{17}$$

Of special significance for this type of flow and heat transfer problem are the mass flow rate in the porous medium channel, the friction factor, and the heat

carried out by the fluid through the porous medium channel. Information on these physical parameters is important for design purposes of channels embedded in porous media. The mass flow rate through the porous medium channel m_p can be calculated as

$$m_p = \int_0^1 U\,dY = B + \frac{D\sin\sqrt{\Pr H} - E(\cos\sqrt{\Pr H} - 1)}{\sqrt{\Pr H}} + \frac{C_3\sinh\sqrt{A+M^2} + C_4\left(\cosh\sqrt{A+M^2} - 1\right)}{\sqrt{A+M^2}} \tag{18}$$

The dimensionless average velocity along the X direction, U_{avg}, in this case is given by

$$U_{avg} = \frac{\bar{u}_p w}{\nu\,\mathrm{Gr}} = \frac{\mathrm{Re}}{\mathrm{Gr}} = m_p \tag{19}$$

Equation (18) gives the mass flow rate in the porous medium channel in terms of the pressure gradient dP/dX, which is included in the constants B, C_3, and C_4. Equation (19) indicates that the pressure gradient can be related to the ratio of Re to Gr. It should be mentioned that in mixed convection problems it is more meaningful to put the physical parameters in terms of the ratio Re/Gr. The limiting cases of free and forced convection are arrived at as $dP/dX \to 0$ and $\mathrm{Re}/\mathrm{Gr} \to \infty$, respectively. It can be shown for a heat-generating fluid that dP/dX is related to Re/Gr as follows:

$$\frac{dP}{dX} = \frac{-(A+M^2)\left(\dfrac{\mathrm{Re}}{\mathrm{Gr}} + \dfrac{D\sinh\sqrt{A+M^2}}{\sqrt{A+M^2}} + \dfrac{C_4^*}{\sqrt{A+M^2}}\left(\cosh\sqrt{A+M^2} - 1\right) - R\right)}{1 - \dfrac{\sinh\sqrt{A+M^2}}{\sqrt{A+M^2}} + \dfrac{\left(\cosh\sqrt{A+M^2} - 1\right)^2}{\sqrt{A+M^2}\sinh\sqrt{A+M^2}}} \tag{20}$$

where

$$C_4^* = \frac{D\left(\cos\sqrt{\Pr H} - \cosh\sqrt{A+M^2}\right) + E\sin\sqrt{\Pr H}}{\sinh\sqrt{A+M^2}}$$

$$R = \frac{D\sin\sqrt{\Pr H} - E(\cos\sqrt{\Pr H} - 1)}{\sqrt{\Pr H}} \tag{21}$$

The friction factor f for mixed convection in a vertical porous medium channel is defined in dimensionless form as

$$f\,\mathrm{Re} = \frac{2\,\mathrm{Gr}}{\mathrm{Re}}\left(\frac{dU}{dY}(0) - \frac{dU}{dY}(1)\right) \tag{22}$$

where $\mathrm{Re} = \bar{u}_p w/\nu$ ($\bar{u}_p$ being the average fluid velocity in the x direction) is the Reynolds number and Gr is the Grashof number and is defined for the different thermal conditions as tabulated in Table 1.

Taking the first derivative of Eq. (16), evaluating the result at $Y = 0$ and $Y = 1$, and substituting into Eq. (22) yields

$$f\,\mathrm{Re} = \frac{2\,\mathrm{Gr}}{\mathrm{Re}}\Big[D\sqrt{\mathrm{Pr}\,H}\,\sin\sqrt{\mathrm{Pr}\,H} + E\sqrt{\mathrm{Pr}\,H}\,(1-\cos\sqrt{\mathrm{Pr}\,H}) - C_3\sqrt{A+M^2}\,\sinh\sqrt{A+M^2} + C_4\sqrt{A+M^2}\,\big(1-\cosh\sqrt{A+M^2}\big)\Big] \tag{23}$$

The heat carried out by the fluid in the porous medium channel for the problem considered is given by

$$\begin{aligned} Q_f &= \int_0^1 U\phi\,dY \\ &= \frac{\cos\sqrt{\mathrm{Pr}\,H}}{A+M^2+\mathrm{Pr}\,H}\Big[\big(C_1C_3\sqrt{A+M^2} - C_2C_4\sqrt{\mathrm{Pr}\,H}\big)\sinh\sqrt{A+M^2} \\ &\qquad + \big(C_1C_4\sqrt{A+M^2} - C_2C_3\sqrt{\mathrm{Pr}\,H}\big)\cosh\sqrt{A+M^2}\Big] \\ &\quad + \frac{\sin\sqrt{\mathrm{Pr}\,H}}{A+M^2+\mathrm{Pr}\,H}\Big[\big(C_1C_3\sqrt{\mathrm{Pr}\,H} + C_2C_4\sqrt{A+M^2}\big)\cosh\sqrt{A+M^2} \\ &\qquad + \big(C_1C_4\sqrt{\mathrm{Pr}\,H} + C_2C_3\sqrt{A+M^2}\big)\sinh\sqrt{A+M^2}\Big] \\ &\quad + \frac{\big(C_2C_3\sqrt{\mathrm{Pr}\,H} - C_1C_4\sqrt{A+M^2}\big)}{A+M^2+\mathrm{Pr}\,H} + \frac{DC_1+EC_2}{2} \\ &\quad + \frac{BC_1}{\sqrt{\mathrm{Pr}\,H}}\sin\sqrt{\mathrm{Pr}\,H} + \left(\frac{DC_1-EC_2}{4\sqrt{\mathrm{Pr}\,H}}\right)\sin(2\sqrt{\mathrm{Pr}\,H}) \\ &\quad - \frac{BC_2}{\sqrt{\mathrm{Pr}\,H}}(\cos\sqrt{\mathrm{Pr}\,H} - 1) - \left(\frac{EC_1+DC_2}{4\sqrt{\mathrm{Pr}\,H}}\right)[\cos(2\sqrt{\mathrm{Pr}\,H}) - 1] \end{aligned} \tag{24}$$

The limiting cases of forced and free convection flow in a porous medium channel in the presence of a magnetic field can be recovered by setting the temperature term ϕ and the pressure gradient dP/dX to zero in the momentum

equation, Eq. (10). Therefore Eqs. (12)–(24) with $B = 0$ are applicable for free convection problems. However, if D and E are formally set to zero in Eqs. (12)–(24), then the solutions for forced convection heat transfer are recovered. In addition, if $M = 0$, the corresponding mixed, free, and forced convection solutions for non-electrically conducting fluids are obtained. It should be mentioned that in the absence of magnetic field and the fluid heat generation effects, Eqs. (12)–(24) are consistent with those reported by Kou and Lu [10]. In addition, if A, H, and M are all formally set to zero, the results of Cheng et al. [25] for fully developed mixed convection in vertical channels will be recovered.

Heat-Absorbing Fluid (Sink)

For such a fluid, the energy equation, Eq. (11), with the negative sign in the second term is solved for ϕ subject to the appropriate thermal boundary conditions to yield

$$\phi = C_5 \cosh \sqrt{\mathrm{Pr}\, H}\, Y + C_6 \sinh \sqrt{\mathrm{Pr}\, H}\, Y \tag{25}$$

where C_5 and C_6 are given by

$$C_5 = \phi_L \qquad C_6 = \frac{\phi_R - \phi_L \cosh \sqrt{\mathrm{Pr}\, H}}{\sinh \sqrt{\mathrm{Pr}\, H}} \tag{26}$$

for isothermal-isothermal boundary conditions

$$C_5 = \phi_L \qquad C_6 = \frac{-Q_R - \phi_L \sqrt{\mathrm{Pr}\, H} \sinh \sqrt{\mathrm{Pr}\, H}}{\sqrt{\mathrm{Pr}\, H} \cosh \sqrt{\mathrm{Pr}\, H}} \tag{27}$$

for isothermal-isoflux boundary conditions, and

$$C_5 = \frac{\phi_R + Q_L/\sqrt{\mathrm{Pr}H} \sinh \sqrt{\mathrm{Pr}\, H}}{\cosh \sqrt{\mathrm{Pr}\, H}} \qquad C_6 = -\frac{Q_L}{\sqrt{\mathrm{Pr}\, H}} \tag{28}$$

for isoflux-isothermal boundary conditions.

The corresponding flow velocity solution can be shown to be

$$U = F + G \cosh \sqrt{\mathrm{Pr}\, H}\, Y + I \sinh \sqrt{\mathrm{Pr}\, H}\, Y + C_7 \cosh \sqrt{A + M^2}\, Y$$
$$+ C_8 \sinh \sqrt{A + M^2}\, Y \tag{29}$$

where

$$F = \frac{-dP/dX}{A + M^2} \qquad G = \frac{-C_5}{\mathrm{Pr}\,H - (A + M^2)} \qquad I = \frac{-C_6}{\mathrm{Pr}\,H - (A + M^2)}$$

$$C_7 = -F - G \qquad C_8 = \frac{C_7 \cosh\sqrt{A + M^2} + F + G\cosh\sqrt{\mathrm{Pr}\,H} + I\sinh\sqrt{\mathrm{Pr}\,H}}{-\sinh\sqrt{A + M^2}} \tag{30}$$

The mass flow rate, the pressure gradient-ratio of Re to Gr relation, the friction factor, and the heat carried out by the fluid for this case take on the respective forms

$$m_p = F + \frac{G\sinh\sqrt{\mathrm{Pr}\,H} + I(\cosh\sqrt{\mathrm{Pr}\,H} - 1)}{\sqrt{\mathrm{Pr}\,H}} + \frac{C_7\sinh\sqrt{A + M^2} + C_8(\cosh\sqrt{A + M^2} - 1)}{\sqrt{A + M^2}} \tag{31}$$

$$\frac{dP}{dX} = \frac{-(A + M^2)\left(\dfrac{\mathrm{Re}}{\mathrm{Gr}} + \dfrac{G\sinh\sqrt{A + M^2}}{\sqrt{A + M^2}} + \dfrac{C_8^*}{\sqrt{A + M^2}}(\cosh\sqrt{A + M^2} - 1) + Z\right)}{1 - \dfrac{\sinh\sqrt{A + M^2}}{\sqrt{A + M^2}} + \dfrac{(\cosh\sqrt{A + M^2} - 1)^2}{\sqrt{A + M^2}\sinh\sqrt{A + M^2}}} \tag{32}$$

where

$$C_8^* = \frac{G(\cosh\sqrt{\mathrm{Pr}\,H} - \cosh\sqrt{A + M^2}) + I\sinh\sqrt{\mathrm{Pr}\,H}}{\sinh\sqrt{A + M^2}} \tag{33}$$

$$Z = \frac{G\sinh\sqrt{\mathrm{Pr}\,H} - I(\cosh\sqrt{\mathrm{Pr}\,H} - 1)}{\sqrt{\mathrm{Pr}\,H}}$$

$$f\,\mathrm{Re} = \frac{2\,\mathrm{Gr}}{\mathrm{Re}}\Big[-G\sqrt{\mathrm{Pr}\,H}\sinh\sqrt{\mathrm{Pr}\,H} + I\sqrt{\mathrm{Pr}\,H}(1 - \cosh\sqrt{\mathrm{Pr}\,H}) - C_7\sqrt{A + M^2}\sinh\sqrt{A + M^2} + C_8\sqrt{A + M^2}(1 - \cosh\sqrt{A + M^2})\Big] \tag{34}$$

$$Q_f = \left(\frac{C_5C_7 + C_6C_8}{2}\right)\left(\frac{\sinh\left(\sqrt{\mathrm{Pr}\,H} + \sqrt{A + M^2}\right)}{\sqrt{\mathrm{Pr}\,H} + \sqrt{A + M^2}}\right)$$

$$+\left(\frac{C_5C_7 - C_6C_8}{2}\right)\left(\frac{\sinh\left(\sqrt{\mathrm{Pr}\,H} - \sqrt{A + M^2}\right)}{\sqrt{\mathrm{Pr}\,H} - \sqrt{A + M^2}}\right)$$

$$+\left(\frac{C_5C_8 + C_6C_7}{2}\right)\left(\frac{\cosh\left(\sqrt{\mathrm{Pr}\,H} + \sqrt{A + M^2}\right) - 1}{\sqrt{\mathrm{Pr}\,H} + \sqrt{A + M^2}}\right)$$

$$+\left(\frac{C_6C_7 - C_5C_8}{2}\right)\left(\frac{\cosh\left(\sqrt{\mathrm{Pr}\,H} - \sqrt{A + M^2}\right) - 1}{\sqrt{\mathrm{Pr}\,H} - \sqrt{A + M^2}}\right)$$

$$+\left(\frac{GC_5 - IC_6}{2}\right)\left(\frac{\sinh(2\sqrt{\mathrm{Pr}\,H})}{2\sqrt{\mathrm{Pr}\,H}}\right)$$

$$+\left(\frac{C_5I + C_6G}{2}\right)\left(\frac{\cosh(2\sqrt{\mathrm{Pr}\,H}) - 1}{2\sqrt{\mathrm{Pr}\,H}}\right) + C_5F\,\frac{\sinh\sqrt{\mathrm{Pr}\,H}}{\sqrt{\mathrm{Pr}\,H}}$$

$$+C_6F\,\frac{(\cosh\sqrt{\mathrm{Pr}\,H} - 1)}{\sqrt{\mathrm{Pr}\,H}} + \left(\frac{GC_5 + IC_6}{2}\right) \tag{35}$$

Again, setting $F = 0$ in Eqs. (25)–(35) gives the free convection solutions, while setting both G and I to zero results in forced convection solutions. Also, setting both M and H to zero obtains the special case solutions reported by Kou and Lu [10] and the results of Cheng et al. [25] if A is also equated to zero.

GRAPHICAL RESULTS AND DISCUSSION

It is difficult to assess the influence of the various physical parameters on the solution from the forms of the closed-form results reported previously. Therefore a representative set of graphical results is presented in Figures 2–10 by numerically evaluating the analytical solutions of the velocity, temperature, and friction factor. It is worth mentioning that if the conditions of the wall heat flux and wall temperature of both sides of the channel are such that $Q_L = Q_R = \phi_L - \phi_R$, then the results obtained for each of the thermal boundary conditions discussed earlier are interrelated, and the results of each case can be derived from the other. Therefore, and to avoid compilation of graphical solutions, only the results associated with the isothermal-isothermal thermal boundary condition will be focused upon, with the exception of a few graphs for the other thermal conditions.

Figures 2 and 3 present typical velocity profiles U normalized to the average velocity U_{avg} for various values of the Hartmann number M. Figure 2 is associated with the case of constant and symmetric wall temperatures, while Figure 3 is concerned with constant and asymmetric (not equal) wall temperatures. Increases

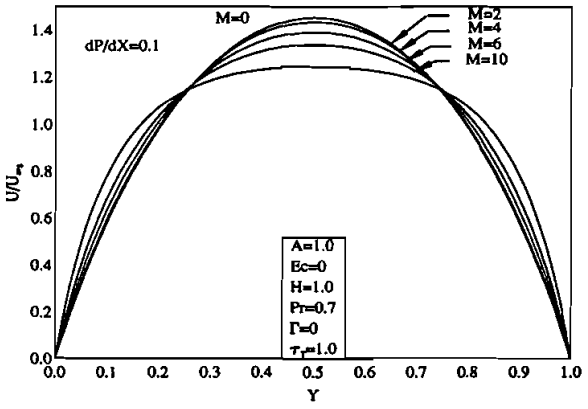

Figure 2. Effects of M on the velocity profiles for the case of constant and symmetric wall temperatures.

in the values of M have a tendency to slow down the movement of the fluid in the porous medium channel. This is because the application of a magnetic field creates a resistive force similar to the drag force, which acts in the opposite direction of the fluid motion, thus causing the velocity (or mass flow rate) of the fluid to decrease. This is depicted in the decreases of the normalized velocity U/U_{avg} as M increases in Figures 2 and 3. It is seen from Figure 2 that the velocity profiles for the case of symmetric wall temperature are symmetric, with the maximum value occurring in the center of the channel, and as M increases, these profiles tend to become more uniform. However, Figure 3 shows that the velocity distributions for the case of asymmetric wall temperatures are not symmetric with respect to the center of the channel and that they become more so as M increases. Greater quantities of the fluid seem to move toward the hot wall of the channel. The same

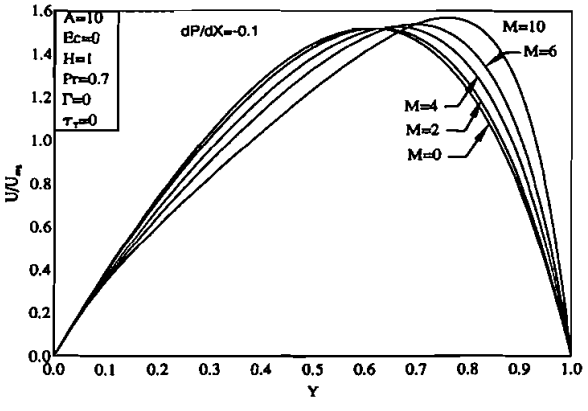

Figure 3. Effects of M on the velocity profiles for the case of constant and asymmetric wall temperatures.

can be said about the influence of the Darcian resistance parameter or the inverse Darcy number A, since similar to M, it represents a resistance to flow. In the absence of magnetic dissipation and axial temperature gradients, the energy equation is independent of the momentum equation. Therefore, the temperature profiles of the fluid are unaffected by changes in the values of M. For this reason, no graphical results for this are presented.

Figures 4 and 5 depict the influence of the heat-generation or absorption coefficient H on the fluid temperature profiles for the cases of symmetric and asymmetric wall temperature conditions, respectively. The negative values of H are associated with cooling of the fluid, while the positive values correspond to the heat generation case or heating of the fluid. It should be noted that, in these and all subsequent figures, the negative signs in the H values are only employed to distinguish between heat generation and heat absorption conditions. As expected, increasing H causes the fluid to become warmer and therefore increases its temperature. For $H = 0$ (no heat generation) the temperature profile is linear, as reported by Kou and Lu [10]. Again, because of the symmetry of the thermal boundary conditions, the temperature profiles are symmetric in Figure 4, while they are nonsymmetric in Figure 5 because of the nonsymmetric nature of the wall temperatures. It is found, from results not presented herein for brevity, that the normalized velocity U/U_{avg} is increased slightly by changes in the values of H.

Figure 6 illustrates the variations of the friction factor f Re that are brought about by simultaneous changes in the inverse Darcy number A and the Hartmann number M. As mentioned above, both the Darcian and the hydromagnetic effects tend to drag or retard the flow in the porous medium channel. This implies that the friction factor increases as a result of increasing A or M or both. This is evident from Figure 6.

Figure 7 presents representative normalized velocity profiles U/U_{avg} for various values of A for the isothermal-isoflux thermal boundary condition case. As mentioned above, increases in the values of A produce reductions in the fluid

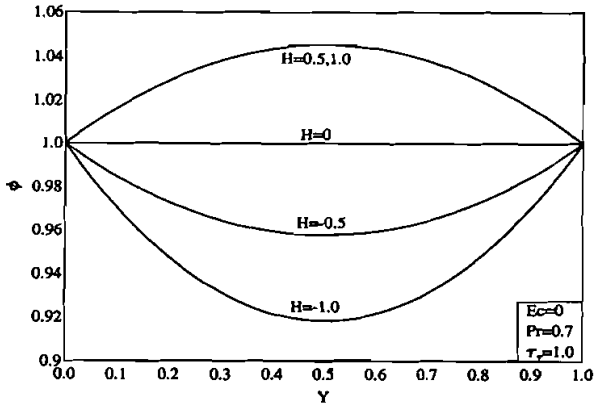

Figure 4. Effects of H on the temperature profiles for symmetric wall temperatures.

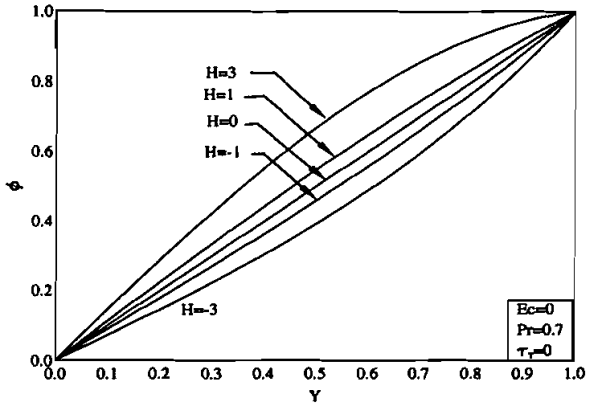

Figure 5. Effects of H on the temperature profiles for asymmetric wall temperatures.

velocity, and its profiles become flatter and more uniform, as shown in Figure 7. The temperature profile is uninfluenced by changes in the values of A, since the energy equation is uncoupled from the momentum equation.

Figure 8 shows typical temperature profiles for various thermal boundary conditions. Curve 1 is obtained for the isothermal-isothermal symmetric condition ($\tau_T = \phi_L/\phi_R = 1$), while curve 2 is associated with the constant asymmetric wall temperatures ($\tau_T = 0$). Curves 3 and 4 correspond to constant isoflux-isothermal ($Q_L = 1$, $\phi_R = 0.5$) and isothermal-isoflux ($\phi_L = 1, Q_R = 0.5$), respectively. It is seen from Figure 8 that all the temperature distributions, which are obtained for the finite heat-generation coefficient ($H = 1$), are not linear, as in the case of no heat generation or absorption ($H = 0$) reported by Kou and Lu [10].

Figures 9 and 10 present typical normalized velocity profiles U/U_{avg} for asymmetric wall temperatures ($\tau_T = 0$) under the influence of various pressure

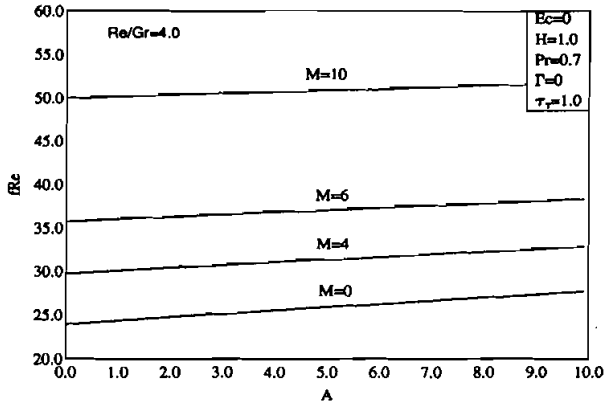

Figure 6. Effects of M and A on the friction factor.

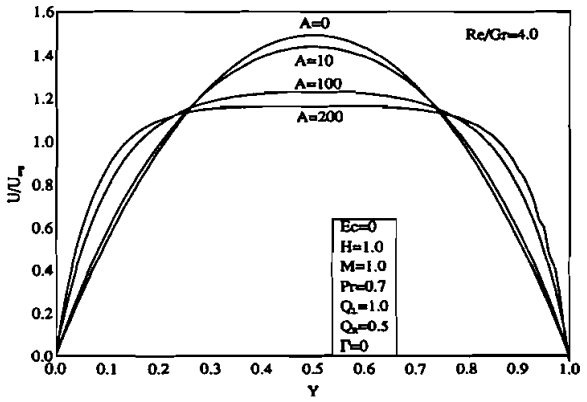

Figure 7. Effects of A on the velocity profiles.

gradients dP/dX and Re/Gr ratios, respectively. The two limiting situations of free and forced convection are attained for $dP/dX = 0$ and as $dP/dX \to -\infty$ (or $\mathrm{Re}/\mathrm{Gr} \to \infty$), respectively. These two limiting solutions are shown clearly in Figure 9. Increases in the values of dP/dX (or decreases in the values of Re/Gr) have the tendency to reduce the mass flow rate in the porous medium channel, and for $\tau_T = 0$, more flow tends to move toward the hot channel surface. It reaches a point where both the pressure and buoyancy forces cause the fluid close to the cold surface to move backward, resulting in a flow reversal condition at large values of dP/dX or small values of Re/Gr. These behaviors are clearly illustrated in Figures 9 and 10. For various degrees of wall temperature asymmetry, the value of dP/dX necessary to cause flow reversal varies. In many flow situations it is very helpful to determine when this condition occurs.

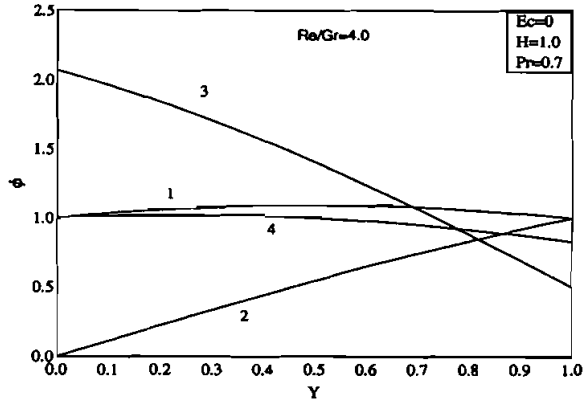

Figure 8. Temperature profiles for various thermal boundary conditions.

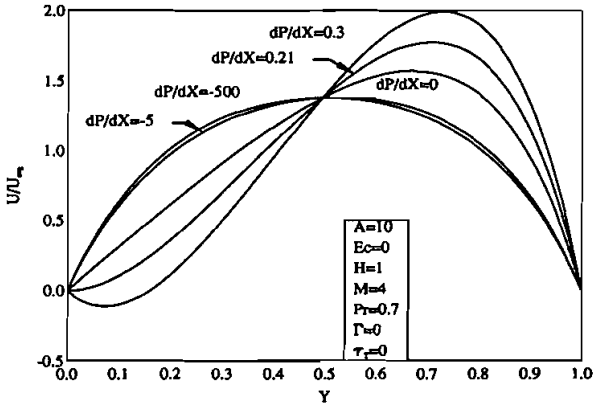

Figure 9. Effects of dP/dX on the velocity profiles.

A backflow or reversal flow zone occurs when the velocity gradients at the left and right walls of the porous medium channel have the same sign. The bounding lines for this zone can be found in terms of the pressure gradient by setting the slopes of the velocity profiles at $Y = 0$ (left wall) and $Y = 1$ (right wall) to zero to obtain

$$\left.\frac{dP}{dX}\right|_{Y=0} = \frac{A + M^2}{1 - \cosh\sqrt{A + M^2}}\left[D\left(\cos\sqrt{\Pr H} - \cosh\sqrt{A + M^2}\right) + E\left(\sin\sqrt{\Pr H} - \sqrt{\frac{\Pr H}{A + M^2}}\sinh\sqrt{A + M^2}\right)\right] \quad (36)$$

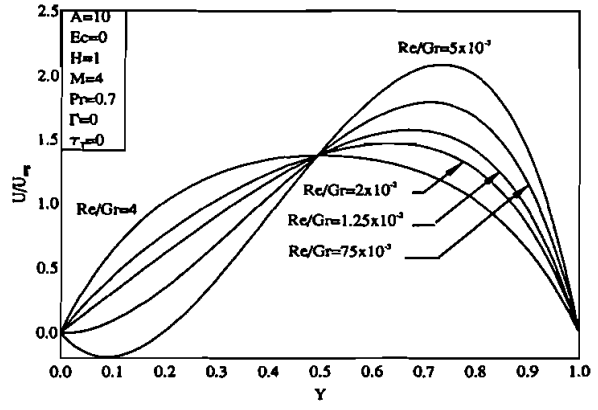

Figure 10. Effects of Re/Gr on the velocity profiles.

$$\left.\frac{dP}{dX}\right|_{Y=1} = \left(\frac{A+M^2}{\sinh\sqrt{A+M^2}}\left\{D\left[\sinh^2\sqrt{A+M^2}+\cosh\sqrt{A+M^2}\left(\cos\sqrt{\mathrm{Pr}\,H}\right.\right.\right.\right.$$

$$\left.\left.\left.\left.-\cosh\sqrt{A+M^2}\right)\right]+E\sin\sqrt{\mathrm{Pr}\,H}\cosh\sqrt{A+M^2}\right\}$$

$$+\sqrt{\mathrm{Pr}\,H(A+M^2)}\left(D\sin\sqrt{\mathrm{Pr}\,H}\right.$$

$$\left.-E\cos\sqrt{\mathrm{Pr}\,H}\right)\Big/\left[\left(1-\cosh\sqrt{A+M^2}\right)\coth\sqrt{A+M^2}\right.$$

$$\left.+\sinh\sqrt{A+M^2}\right] \tag{37}$$

for a heat-generating fluid, and

$$\left.\frac{dP}{dX}\right|_{Y=0} = \frac{A+M^2}{1-\cosh\sqrt{A+M^2}}\left[G\left(\cosh\sqrt{\mathrm{Pr}\,H}-\cosh\sqrt{A+M^2}\right)\right.$$

$$\left.+I\left(\sinh\sqrt{\mathrm{Pr}\,H}-\sqrt{\frac{\mathrm{Pr}\,H}{A+M^2}}\sinh\sqrt{A+M^2}\right)\right] \tag{38}$$

$$\left.\frac{dP}{dX}\right|_{Y=1} = \left(\frac{A+M^2}{\sinh\sqrt{A+M^2}}\left\{G\left[\sinh^2\sqrt{A+M^2}+\cosh\sqrt{A+M^2}\left(\cos\sqrt{\mathrm{Pr}\,H}\right.\right.\right.\right.$$

$$\left.\left.\left.\left.-\cosh\sqrt{A+M^2}\right)\right]+I\sinh\sqrt{\mathrm{Pr}\,H}\cosh\sqrt{A+M^2}\right\}$$

$$-\sqrt{\mathrm{Pr}\,H(A+M^2)}\left(G\sinh\sqrt{\mathrm{Pr}\,H}\right.$$

$$\left.-I\cosh\sqrt{\mathrm{Pr}\,H}\right)\Big/\left[\left(1-\cosh\sqrt{A+M^2}\right)\coth\sqrt{A+M^2}\right.$$

$$\left.+\sinh\sqrt{A+M^2}\right] \tag{39}$$

for a heat-absorbing fluid.

Figure 11 reports the pressure gradient dP/dX, which causes flow reversal at the cold wall of the isothermal-isothermal asymmetric wall temperatures case for different values of the left to right temperature ratio τ_T. For each parametric case indicated by the number attached to the lines and the conditions given in Table 2 there is a reversal flow zone bounded by the two lines having the same number and intersecting at $\tau_T = 1$. It should be mentioned that the bottom line of each case is obtained by evaluating Eq. (36) for heat generation or Eq. (38) for heat absorption, while the upper line is calculated from Eq. (37) for heat generation or Eq. (39) for heat absorption. Upon inspection of the different cases shown, it can be concluded that the presence of the magnetic field or the heat generation effect or both results in increasing the region of backflow or the reversal flow zone. It is also noticed that

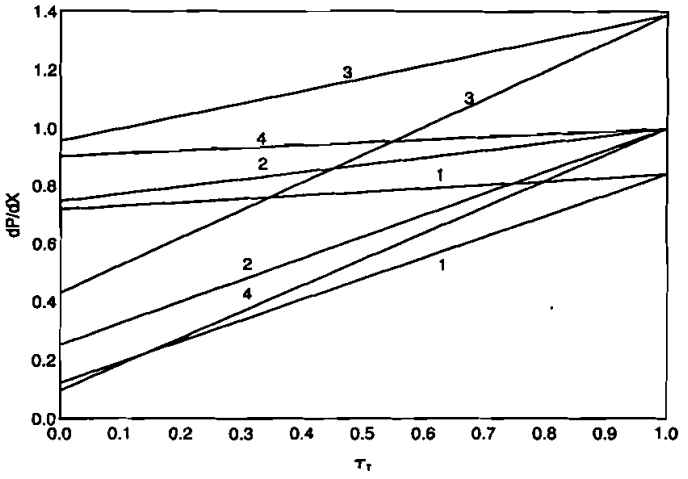

Figure 11. Reversal flow zones for various asymmetric wall temperatures.

no backflow condition occurs for symmetric wall temperatures $\tau_T = 1$. However, as τ_T is decreased from unity, a stronger buoyant effect near the hot wall occurs, which makes the flow at the cold wall move backward. For this type of problem the region above the upper line of each case is called the buoyancy-resisted flow region and the region below is called the buoyancy-assisted flow region, which is considered in the present work. It should be mentioned that there appears to be a mistake in the evaluation of the upper line of the work reported by Kou and Lu [10], since at $\tau_T = 0$, the result should be 0.748 and not 0.5.

Figure 12 depicts the influence of dP/dX and H on the mass flow rate m_p. As expected, the values of m_p decrease as dP/dX increases and they increase as H increases. Figures 13 and 14 present the influences of H and Re/Gr on the heat carried out by the fluid Q_f for various isothermal-isothermal thermal boundary conditions, receptively. It is obvious that as the mass flow rate of the fluid in the channel increases, the heat it carries with it also increases. In addition, as the degree of wall temperature asymmetry increases, the zone of flow reversal decreases, causing higher mass flow rates in the channel. This has the direct effect of

Table 2. Parametric conditions for Figure 11 at $A = 10$, Ec = 0, Pr = 0.7, and $\Gamma = 0$

Line in Figure 11	H	M
1	−5	4
2	0	0
3	5	0
4	0	10

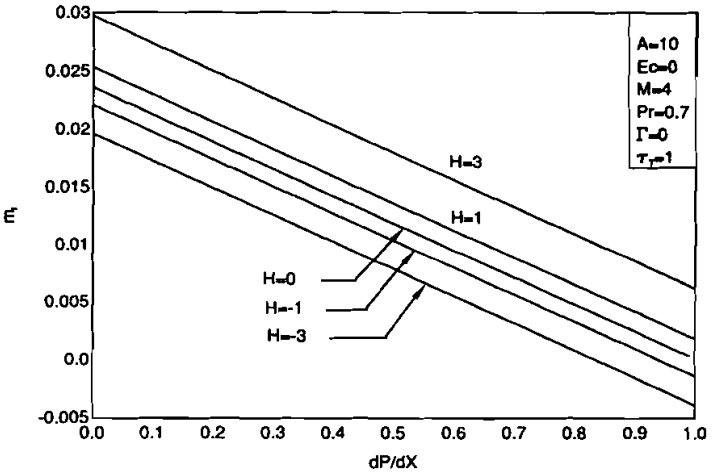

Figure 12. Effects of H and dP/dX on the mass flow rate.

increasing Q_f. These predictions are evident from Figure 13. Furthermore, Eq. (19) shows that the ratio $\mathrm{Re}/\mathrm{Gr}/m_p$. This explains the increases in Q_f shown in Figure 14 as Re/Gr increases.

Table 3 presents a comparison between the values of dP/dX and Q_f obtained from the closed-form solutions reported herein for Pr = 0.7 and those reported by Kou and Lu [10] for Ec = 0, $H = 0$, $M = 0$, and $\Gamma = 0$. It is clear from this table that an excellent agreement exists between these results.

Equations (6)–(9) are nonlinear coupled differential equations and conditions that must be solved numerically, since they exhibit no analytical solution. An implicit iterative tridiagonal finite difference numerical method similar to that discussed by Blottner [26] is employed for this purpose. Equations (6) and (7) are

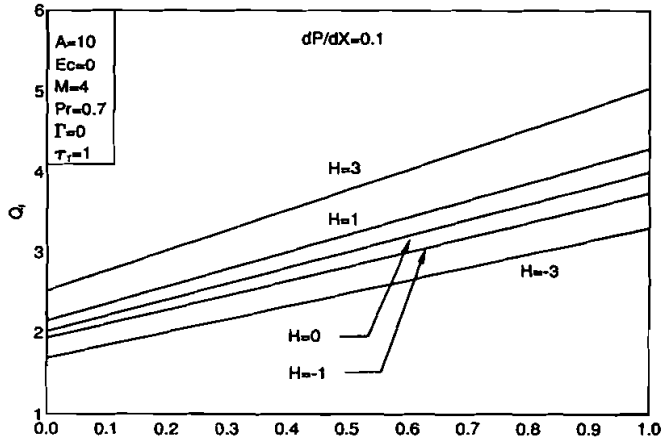

Figure 13. Effects of H and τ_T on the heat flux.

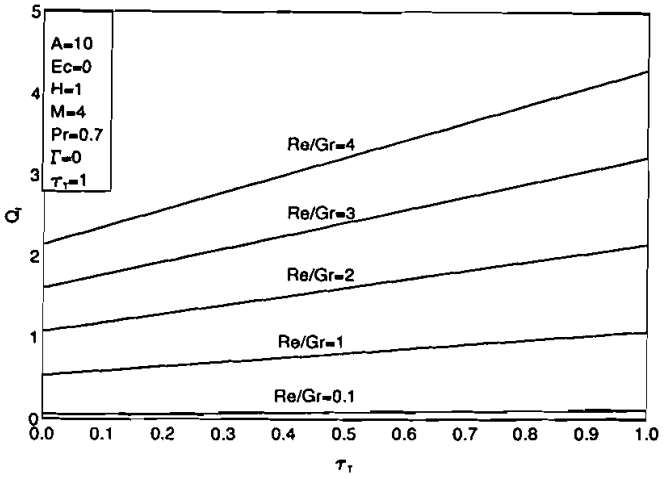

Figure 14. Effects of Re/Gr and τ_T on the heat flux.

discretized using three-point central difference quotients with the first-order derivative of ϕ with respect to X replaced by a two-point backward difference formula. With this, the differential equations are converted into a set of algebraic equations that are solved with iteration (to deal with the nonlinearities of the governing equations) by the Thomas' algorithm (see [26]). Constant step sizes in Y ($\Delta Y = 0.05$) and variable step sizes in X ($\Delta X_1 = 0.001$ and a growth factor of 1.03) are employed in the present work. These values were arrived at after many numerical experimentations were performed to assess grid independence. A convergence criterion based on the relative difference between two successive iterations (set to 10^{-5} in the present work) was employed. The correctness of the numerical method was tested using the closed-form results reported earlier. In general, it is found that the effect of Γ on the velocity distribution in the channel is very similar to that of A and M, namely, it causes U/U_{avg} to decrease as it increases. More numerical results for the friction factor, the mass flow rate, and the convective heat carried out by the fluid are presented in Table 4.

Table 3. Comparison with the results of Kou and Lu [10] at Ec = 0, Pr = 0.7, and $\Gamma = 0$

Re/Gr	A	H	M	dP/dX	dP/dX [10]	Q_f	Q_f [10]	f Re	τ_T
4.0	0	0	0	−46.668	—	4.526	—	23.834	1.0
	1	0	0	−51.794	−51.794	4.000	4.000	24.397	1.0
	10	0	0	−94.485	−94.480	4.000	4.000	27.743	1.0
0.3	10	0	0	−6.161	−6.161	0.300	0.300	27.743	1.0
	10	0	1	−6.514	—	0.300	—	28.092	1.0
	10	1	1	−6.439	—	0.322	—	28.013	1.0
	10	−1	1	−5.726	—	0.264	—	24.971	1.0
4.0	100	0	0	−499.294	−499.240	3.007	3.000	49.969	0.5
	100	0	0	−499.543	−499.490	2.002	2.000	50.031	0
	100	1	1	−503.551	—	3.212	—	50.159	0.5

Table 4 shows the influence of the porous medium inertia coefficient Γ on $f\,\mathrm{Re}/\mathrm{Re}/\mathrm{Gr} = f\,\mathrm{Gr}$, m_p, and Q_f. As expected, it is observed that both m_p and Q_f decrease and $f\,\mathrm{Gr}$ increases as Γ increases. This is due to the increased flow resistance that the porous medium inertia coefficient adds.

It should be mentioned that all the closed-form and numerical results associated with $H = 0$ (neutral fluid) and $M = 0$ (no magnetic field) reported herein are in excellent agreement with the solutions reported by Kou and Lu [10] and those given by Cheng et al. [25] for $H = 0$, $M = 0$, and in the absence of the porous medium. The results reported in the present article can be best validated by direct comparison with available experimental data. However, this is not done herein, since these data appear to be lacking at present.

CONCLUSION

Continuum equations were developed governing steady, laminar, fully developed, hydromagnetic, non-Darcian mixed convection flow of an electrically conducting and heat-generating/absorbing fluid in a channel embedded in a uniform porous medium. Proper dimensionless parameters were employed for various thermal boundary conditions on the left and right walls of the channel prescribed as isothermal-isothermal, isothermal-isoflux, and isoflux-isothermal. The governing equations accounted for such effects as boundary and inertia effects of porous media, buoyancy effects, and heat generation/absorption and hydromagnetic effects. In the absence of porous medium inertial effects, magnetic dissipation, and temperature gradient in the flow direction, the governing equations were solved analytically for both heat generation and heat absorption cases and the different thermal boundary conditions mentioned above. Analytical expressions were developed for the velocity and temperature profiles in the channel as well as for the mass flow rate, friction factor, and heat carried out by the fluid in the channel. Conditions for the occurrence of fluid-reversed flow zones were reported. The fully nonlinear governing equations were solved numerically by an implicit tridiagonal finite difference method. Favorable comparisons with the obtained analytical results and previously published work were performed. No comparisons with experimental work was made, since these data appear to be lacking at present. Graphical results of the closed-form and numerical results were reported for various parametric conditions to illustrate special features of the solution. It is found that the presence of either the magnetic field or the heat generation effect or both causes the region of the assured reversed flow zone to increase for

Table 4. Values of $f\,\mathrm{Gr}$, m_p, and Q_f for various parametric conditions at $A = 10$, $\mathrm{Ec} = 1.0$, $H = 1.0$, $M = 1.0$, and $\mathrm{Pr} = 0.7$

Γ	dP/dX	$f\,\mathrm{Gr}$	m_p	Q_f	τ_T
10	0.1	0.8850	0.0296	0.0253	1.0
100	0.1	0.8326	0.0267	0.0233	1.0
10	−0.1	1.0769	0.0359	0.0295	1.0
10	−0.1	0.8586	0.0291	0.0189	0.5

asymmetric wall temperatures. No reversal flow occurs for the case of symmetric wall temperatures. It is hoped that the analytical and numerical results reported here will serve as a vehicle for validating computer routines for more complex mixed convection problems and stimulate interest for experimental work.

REFERENCES

1. E. M. Sparrow and R. D. Cess, Effect of Magnetic Field on Free Convection Heat Transfer, *Int. J. Heat Mass Transfer*, vol. 3, pp. 267–274, 1961.
2. N. Riley, Magnetohydrodynamics Free Convection, *J. Fluid Mech.*, vol. 18, pp. 577–586, 1964.
3. R. Gulab and R. Mishra, Unsteady Flow Through Magnetohydrodynamic Porous Media, *Indian J. Pure Appl. Math.*, vol. 8, pp. 637–642, 1977.
4. A. Raptis and N. Kafoussias, Heat Transfer in Flow Through a Porous Medium Bounded by an Infinite Vertical Plane Under the Action of a Magnetic Field, *Energy Res.*, vol. 6, pp. 241–245, 1982.
5. A. Raptis and A. K. Singh, MHD Free Convection Flow Past an Accelerated Vertical Plate, *Int. Commun. Heat Mass Transfer*, vol. 10, pp. 313–321, 1983.
6. A. A. Raptis, Flow Through a Porous Medium in the Presence of a Magnetic Field, *Energy Res.*, vol. 10, pp. 97–100, 1986.
7. J. P. Garandet, T. Alboussiere, and R. Moreau, Buoyancy Driven Convection in a Rectangular Enclosure with a Transverse Magnetic Field, *Int. J. Heat Mass Transfer*, vol. 35, pp. 741–749, 1992.
8. M. A. Hossain, Viscous and Joule Heating Effect on MHD-Free Convection with Variable Plate Temperture, *Int. J. Heat Mass Transfer*, vol. 35, pp. 3485–3487, 1992.
9. N. G. Kafoussias, MHD Free Convection Flow Through a Nonhomogeneous Porous Medium over an Isothermal Cone Surface, *Mech. Res. Commun.*, vol. 19, pp. 89–94, 1992.
10. H. S. Kou and K. J. Lu, Combined Boundary and Inertia Effects for Fully Developed Mixed Convection in a Vertical Channel Embedded in Porous Media, *Int. Commun. Heat Mass Transfer*, vol. 20, 333–345, 1993.
11. N. C. Sacheti, P. Chamdran, and A. K. Singh, An Exact Solution for Unsteady Magnetohydrodynamics Free Convection Flow with Constant Heat Flux, *Int. Commun. Heat Mass Transfer*, vol. 21, pp. 131–142, 1994.
12. H. S. Takhar and P. C. Ram, Magnetohydrodynamics Free Convection Flow of Water at 40°C Through a Porous Medium, *Int. Commun. Heat Mass Transfer*, vol. 21, pp. 371–376, 1994.
13. T. K. Aldoss, T. S. Chen, and B. F. Armaly, Mixed Convection over Nonisothermal Horizontal Surfaces in a Porous Medium—The Entire Regime, *Int. J. Heat Mass Transfer*, vol. 25, pp. 685–701, 1994.
14. A. J. Chamkha, Transient Power-Law Fluid Flow in a Porous Medium Channel, *Fluid/Particle Separation J.*, vol. 7, pp. 4–7, 1994.
15. A. J. Chamkha, Unsteady Hydromagnetic Natural Convection in a Fluid-Saturated Porous Medium Channel, *Adv. Filtration Separation Technol.*, vol. 10, pp. 369–375, 1996.
16. W. J. Minkowycz, P. Cheng, and R. N. Hirschberg, Nonsimilar Boundary Layer Analysis of Mixed Convection About a Horizontal Heated Surface in a Fluid-Saturated Porous Medium, *Int. Commun. Heat Mass Transfer*, vol. 11, pp. 127–141, 1984.
17. W. J. Minkowycz, P. Cheng, and C. H. Chang, Mixed Convection About a Nonisothermal Cylinder and Sphere in a Porous Medium, *Numer. Heat Mass Transfer*, vol. 8, pp. 349–359, 1985.

18. K. Vafai and C. L. Tien, Boundary and Inertia Effects on Flow and Heat Transfer in Porous Media, *Int. J. Heat Mass Transfer*, vol. 24, pp. 195–203, 1981.
19. K. Vafai and C. L. Tien, Boundary and Inertia Effects on Convective Mass Transfer in Porous Media, *Int. J. Heat Mass Transfer*, vol. 25, pp. 1183–1190, 1982.
20. J. T. Hong, Y. Yamada, and C. L. Tien, Effects of Non-Darcian and Nonuniform Porosity on Vertical-Plate Natural Convection in Porous Media, *ASME J. Heat Transfer*, vol. 109, pp. 356–362, 1987.
21. O. A. Plumb and J. C. Huenefeld, Non-Darcy Natural Convection from Heated Surfaces in Saturated Porous Media, *Int. J. Heat Mass Transfer*, vol. 24, pp. 765–768, 1981.
22. K. Vajravelu and A. Hadjinicolaou, Heat Transfer in a Viscous Fluid over a Stretching Sheet with Viscous Dissipation and Internal Heat Generation, *Int. Commun. Heat Mass Transfer*, vol. 20, pp. 417–430, 1993.
23. K. Vajravelu and J. Nayfeh, Hydromagnetic Convection at a Cone and a Wedge, *Int. Commun. Heat Mass Transfer*, vol. 19, pp. 701–710, 1992.
24. A. J. Chamkha, Non-Darcy Hydromagnetic Free Convection from a Cone and a Wedge in Porous Media, *Int. Commun. Heat Mass Transfer*, vol. 23, pp. 875–887, 1996.
25. C. H. Cheng, H. S. Kou, and W. H. Huang, Flow Reversal and Heat Transfer of Fully Developed Mixed Convection in Vertical Channels, *AIAA J. Thermophys.*, vol. 4, no. 3, pp. 375–383, 1990.
26. F. Blottner, Finite Difference Methods of Solutions of the Boundary-Layer Equations, *AIAA J.*, vol. 8, pp. 193–205, 1970.